Multimode Network Description of a Planar Periodic Metal-Strip Grating at a Dielectric Interface—Part II: Small-Aperture and Small-Obstacle Solutions

MARCO GUGLIELMI AND ARTHUR A. OLINER, LIFE FELLOW, IEEE

Abstract—**In Part I of this pair of papers, we developed new multimode equivalent network representations for the scattering of a plane wave incident on a metal-strip grating at an air–dielectric interface. The analytical phrasing led to two Fredholm integral equations of the first kind with singular kernels. In this paper (Part II) we present two analytical small-argument solution procedures for those integral equations, and we derive explicit expressions for the elements of the coupling matrices in the small-aperture and small-obstacle ranges for both TE and TM polarizations. Simple and useful equivalent network descriptions are derived in which all of the network elements are in very simple analytical form. When the discontinuity is "electrically small," the resulting network becomes dramatically simple. The various networks are discussed together with estimates for their ranges of applicability. Finally, numerical comparisons are presented with an independent numerical reference solution, showing that the new simple networks are indeed very accurate within their ranges of applicability.**

I. Introduction

IN PART I of this set of two papers, we presented two general formal integral-equation solutions to the problem of a plane wave incident at an angle under multimode conditions on a metal-strip grating located at an air–dielectric interface, as shown in Fig. 1. The solutions were developed in terms of equivalent networks with a shunt matrix coupling the various modes (spectral orders) excited by the grating. For each solution, the generic coupling matrix element $A_{m,n}$ (defined in (3) below) was given in terms of the integral of an unknown function specified by a partial integral equation. It was also shown that although we actually formulated the problem for both TE and TM polarizations from two different viewpoints, namely, aperture and obstacle formulations, we need to solve only two types of integral equation, corresponding respectively to the "electrically small" and "electrically large" discontinuities, to have the solutions for all four cases.

Manuscript received March 8, 1988; revised August 31, 1988. This work was supported by the Joint Services Electronics Program under Contract F49620-85-C-0078.

M. Guglielmi was with the Weber Research Institute, Polytechnic University, Brooklyn, NY. He is now with the Electrical Engineering Department, New Jersey Institute of Technology, Newark, NJ 07102.

A. A. Oliner is with the Weber Research Institute, Polytechnic University, 333 Jay Street, Brooklyn, NY 11201.

IEEE Log Number 8825385.

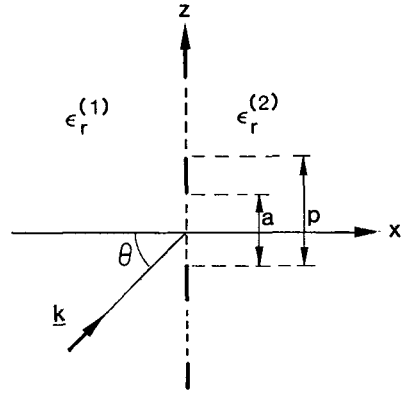

Fig. 1. Plane wave incident at an arbitrary angle on a metal-strip grating at a plane air–dielectric interface, where the grating period permits propagating higher spectral orders. Both TE and TM polarizations are considered.

In this paper, we present two analytical methods for solving those integral equations in the small-argument range; for both the electrically small and the electrically large cases, simple and accurate equivalent network descriptions are derived in which all of the network elements are in very simple analytical form. For the electrically small case, the resulting network turns out to be *dramatically simple* for both TE and TM excitations. The interesting properties of these networks are discussed, and it is shown how their ranges of validity can be assessed for each case. Finally, several numerical computations are presented that show, via comparisons with values obtained from an accurate independent reference solution, how these new network descriptions are indeed useful and accurate over a reasonably wide range of parameter values.

Before proceeding with the exposition of the solution procedures, it is convenient to recall the two equations in question, which are both Fredholm integral equations of the first kind with singular kernels. The first type of integral equation, hereafter referred to as F1, is

$$e^{-j\frac{2n\pi}{p}z} = \int_{-b/2}^{b/2} f_n(z')\, B \sum_{m\neq 0} \frac{e^{-j\frac{2m\pi}{p}(z-z')}}{|m|}\, dz' \qquad (1)$$

and it applies to the aperture formulation with TM excitation or the obstacle formulation with TE excitation, corresponding to the "electrically large" case. The second type, hereafter referred to as F2, is

$$e^{-j\frac{2n\pi}{p}z} = \int_{-b/2}^{b/2} f_n(z') B \sum_{m\neq 0} |m| e^{-j\frac{2m\pi}{p}(z-z')}\, dz' \quad (2)$$

which is valid for the obstacle formulation with TM excitation or the aperture formulation with TE excitation, corresponding to the "electrically small" case. Finally, the integral relation between the generic matrix element $A_{m,n}$ and the unknown function $f_n(z)$ is

$$A_{m,n} = \int_{-b/2}^{b/2} f_n(z') e^{j\frac{2m\pi}{p}z'}\, dz'. \quad (3)$$

Expressions (1) and (2) correspond to (48) and (49) of Part I, respectively, whereas (3) corresponds to either (15) or (35) of Part I, depending on whether $A_{m,n}$ refers to $Z_{m,n}$ or $Y_{m,n}$. Note that, to simplify notation, we have dropped the superscripts on B and $f_n(z')$ in (1) and (2).

II. Small-Argument Analytical Solution of F1: The First Integral Equation

In this section, we outline a solution procedure for the F1 integral equation derived in Part I that yields a very simple and accurate "small-argument" approximate result. This solution procedure has already been used by Palocz and Oliner [1], in a form that is basically an extension to a multimoded situation of the discussion presented in the *Waveguide Handbook* [2] for a single propagating mode. This procedure is briefly outlined here for the sake of clarity. To illustrate the above-mentioned procedure, let us examine the relevant integral equation (1) and note that its kernel can be summed in closed form according to [3], obtaining

$$K(z) = 2\sum_{m=1}^{\infty} \frac{1}{m}\cos\frac{2m\pi}{p}z = -2\ln\left|2\sin\frac{\pi}{p}z\right|. \quad (4)$$

Therefore, substituting (4) into (1) and expanding the sine function, we obtain

$$e^{-j\frac{2n\pi}{p}z} = \int_{-b/2}^{b/2} f_n(z') \cdot(-2B)\ln\left|2\sin\frac{\pi}{p}z\cos\frac{\pi}{p}z' - 2\cos\frac{\pi}{p}z\sin\frac{\pi}{p}z'\right| dz'. \quad (5)$$

The main difficulty in solving (5) is due to the fact that the period p of the kernel is different from the interval b of integration. These lengths p and b are defined in the coordinate system shown in Fig. 2, where the interval $-b/2$ to $b/2$ represents the aperture width a in Fig. 1 if the formulation of the problem is made in aperture terms, or the width of the obstacle ($p-a$ in Fig. 1) if an obstacle formulation is used. This difficulty can be overcome with a shift of the origin to that shown in Fig. 3 and then by the introduction of a change of variables due to Schwinger [4]:

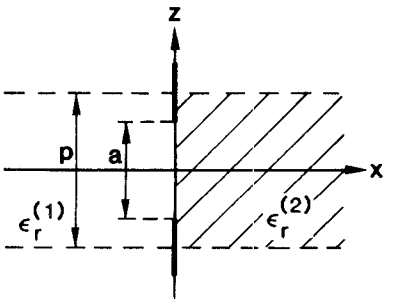

Fig. 2. The original coordinate system for both the "electrically large" and the "electrically small" phrasings of the scattering problem.

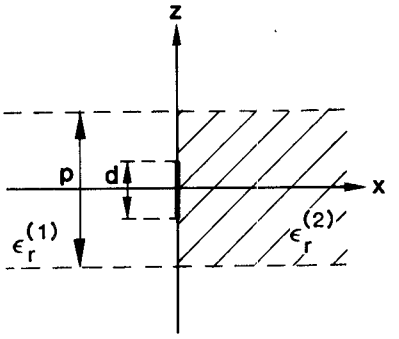

Fig. 3. The new coordinate system introduced in connection with (6) and (7) for the small-argument solution of the integral equation relevant to the "electrically large" case.

$$\cos\frac{\pi}{p}z = \alpha\cos\theta \quad (6)$$

$$\alpha = \sin\frac{\pi}{2}\frac{b}{p}. \quad (7)$$

Using the coordinate system shown in Fig. 3 and the proposed change of variables, we have

$$z = \frac{-b}{2} \rightarrow z = d_1 \rightarrow \theta = 0 \quad (8)$$

$$z = \frac{b}{2} \rightarrow z = d_2 \rightarrow \theta = \pi. \quad (9)$$

In (5), however, we also have sine terms, which can be easily rewritten in terms of cosines. The kernel can then be expanded in terms of α, following the treatment in [1]; when we retain terms only up to the second order, it becomes

$$\frac{-1}{2}K(\theta,\theta') = \ln\alpha - 2\sum_{m=1}^{\infty}\frac{\sin m\theta \sin m\theta'}{m} - \frac{\alpha^2}{2}\cos\theta\cos\theta' + O(\alpha^4). \quad (10)$$

Now that we have expressed the kernel in a more convenient form, we expand the left-hand side of (5) in terms of α, obtaining

$$e^{-j\frac{2n\pi}{p}z} \rightarrow (-1)^n\{1 + 2nj\alpha\cos\theta - 2n^2\alpha^2\cos^2\theta + O(\alpha^3)\} \quad (11)$$

where we have introduced the change of variables shown in (6) and (7).

The next step is the expansion of the unknown function $f_n(z')$ in (5), together with the necessary mapping derivative, in a similar power series:

$$\left[f_n(z')\frac{dz'}{d\theta'}\right] \approx M_n^{R,0}(\theta') + j\alpha M_n^{I,1}(\theta') + \alpha^2 M_n^{R,2}(\theta') \tag{12}$$

where M_n^R and M_n^I are the real and imaginary parts of $f_n(z')\,dz'/d\theta'$. Finally, employing (10), (11), and (12) in (5) and comparing like coefficients, we obtain the results

$$\int_0^{\pi} M_n^{I,1}(\theta')\cos\theta'\,d\theta' = \frac{(-1)^{n+1}2n}{-4B} \tag{13}$$

$$\int_0^{\pi} M_n^{R,0}(\theta')\,d\theta' = \frac{(-1)^n}{-2B\ln\alpha} \tag{14}$$

$$\int_0^{\pi} M_n^{R,2}(\theta')\,d\theta' = \frac{(-1)^{n+1}n^2}{-2B\ln\alpha} \tag{15}$$

$$\int_0^{\pi} M_n^{R,2}(\theta')\cos 2\theta'\,d\theta' = \frac{(-1)^{n+1}n^2}{2B}. \tag{16}$$

The above integrals can now be used to evaluate the generic matrix element $A_{m,n}$ given by

$$A_{m,n} = \int_{-b/2}^{b/2} f_n(z)\,e^{j\frac{2m\pi}{p}z}\,dz \tag{17}$$

which then becomes

$$A_{m,n} \approx \frac{(-1)^{m+n+1}}{2B\ln\alpha}\left[1-\alpha^2(m^2+n^2)-2\alpha^2 mn\ln\alpha\right], \qquad m,n = 0,\pm1,\pm2,\cdots \tag{18}$$

$$\alpha = \sin\frac{\pi}{2}\frac{b}{p} \tag{19}$$

where, to carry out the evaluation of the integral, we have used the same change of variable and expansions introduced earlier. Equations (18) and (19) constitute the "small-argument" solution of (1). To recover the solution for a specific scattering problem, we need only to use the appropriate expressions for the constants b and B defined in Section V of Part I.

III. Small-Argument Analytical Solution of F2: The Second Integral Equation

In this section we present a novel analytical approximate solution of the F2 integral equation derived in Part I. The basic idea behind this procedure is the reduction of the relevant integral equation to the canonical form of the Cauchy integral equation that has a known solution.

The first step is to rewrite the kernel of (2) in the form

$$K(z-z') = \lim_{\delta\to 0}\sum_{m\neq 0}|m|e^{-\delta|m|}e^{-j\frac{2m\pi}{p}(z-z')} \tag{20}$$

to aid in summing the kernel in closed form. This phrasing is in principle equivalent to formulating the integral equation a small distance δ away from the grating in the x direction and then taking the limit for $\delta\to 0$. Next, we substitute (20) into (2) and, integrating by parts, obtain

$$e^{-j\frac{2n\pi}{p}z} = \int_{-b/2}^{b/2} f_n'(z')\frac{B}{-j\frac{2\pi}{p}} \cdot \lim_{\delta\to 0}\sum_{m\neq 0}\frac{|m|}{m}e^{-\delta|m|}e^{-j\frac{2m\pi}{p}(z-z')}\,dz' \tag{21}$$

together with the condition

$$f_n(z')|_{z'=\pm b/2} = 0 \tag{22}$$

which is consistent with the boundary conditions for both TE and TM excitations. The kernel of (21) can now be summed in closed form by recalling that [3]

$$\sum_{m=1}^{\infty} e^{-\delta m}\sin mx = \frac{1}{2}\frac{\sin x}{\cosh\delta - \cos x}. \tag{23}$$

Taking the limit for $\delta\to 0$ we can finally express (21) in the more convenient form

$$e^{-j\frac{2n\pi}{p}z} = \int_{-b/2}^{b/2} f_n'(z')\frac{Bp}{2\pi}\frac{\sin\frac{2\pi}{p}(z-z')}{1-\cos\frac{2\pi}{p}(z-z')}\,dz'. \tag{24}$$

The next step is the introduction of the change of variables

$$z = \frac{b}{2}\xi \tag{25}$$

so that, expanding both the kernel and the known function in (24) in a power series in b/p and retaining terms only up to the second order, we can write

$$g_n(\xi) = \frac{1}{\pi}\int_{-1}^{1} F_n(\xi')\frac{d\xi'}{(\xi-\xi')} \tag{26}$$

where

$$g_n(\xi) = 1 - j\pi\frac{b}{p}n\xi - \frac{1}{2}n^2\left(\pi\frac{b}{p}\right)^2\xi^2 \tag{27}$$

$$F_n(\xi) = f_n'\left(\frac{b}{2}\xi\right)\frac{Bp^2}{2\pi}. \tag{28}$$

We now recognize that we have successfully reduced the original integral equation (2) to the canonical form of the Cauchy integral equation. The solution of (26) can now be written at once [5] in the form

$$F_n(\xi) = \frac{1}{\sqrt{1-\xi^2}}\left[C + \frac{1}{\pi}\oint_{-1}^{1}\frac{\sqrt{1-\zeta^2}}{\zeta-\xi}g_n(\zeta)\,d\zeta\right] \tag{29}$$

where the star on the integral sign means that we take its principal value. Equation (29) is the small-argument solution of the original integral equation. The only thing that is

left is the evaluation of constant C; in order to do so, let us recall condition (22) imposed on $f_n(z)$, which is equivalent to

$$\int_{-1}^{1} f_n'\left(\frac{b}{2}\xi\right)\frac{b}{2}\,d\xi = 0. \tag{30}$$

We can now use (28), (29), and (30) to obtain, in a few simple steps,

$$C = -\frac{D_n}{D_0} \tag{31}$$

where

$$D_0 = \int_{-1}^{1} \frac{d\xi}{\sqrt{1-\xi^2}} \tag{32}$$

$$D_n = \int_{-1}^{1} \frac{G_n(\xi)}{\sqrt{1-\xi^2}}\,d\xi \tag{33}$$

$$G_n(\xi) = \frac{1}{\pi}\,\text{⨍}\!\!\!\!-_{-1}^{1} \frac{\sqrt{1-\zeta^2}\,g_n(\zeta)}{\zeta-\xi}\,d\zeta. \tag{34}$$

Having formally evaluated C, we can rewrite the expression for $f_n'\left(\frac{b}{2}\xi\right)$ in the form

$$f_n'\left(\frac{b}{2}\xi\right) \approx \frac{2\pi}{Bp^2}\left\{-\frac{D_n}{D_0\sqrt{1-\xi^2}} + \frac{G_n(\xi)}{\sqrt{1-\xi^2}}\right\}. \tag{35}$$

To recover the function $f_n\left(\frac{b}{2}\xi\right)$ we can now integrate (35), yielding

$$f_n\left(\frac{b}{2}\xi\right) \approx \frac{\pi d}{Bp^2}\left[-\frac{D_n}{D_0}\int_{-1}^{\xi}\frac{d\zeta}{\sqrt{1-\zeta^2}} + \int_{-1}^{\xi}\frac{G_n(\zeta)}{\sqrt{1-\zeta}}\,d\zeta\right]. \tag{36}$$

Equation (36) is, therefore, the approximate analytical solution we are seeking. To obtain the generic impedance element $A_{m,n}$ we need to perform one more integration, namely,

$$A_{m,n} = \int_{-b/2}^{b/2} f_n(z)\,e^{j\frac{2m\pi}{p}z'}\,dz'. \tag{37}$$

Using the notation introduced earlier, together with the following definitions:

$$D_0(\xi) = \int_{-1}^{\xi}\frac{d\zeta}{\sqrt{1-\zeta^2}} \tag{38}$$

$$D_n(\xi) = \int_{-1}^{\xi}\frac{G_n(\zeta)}{\sqrt{1-\zeta^2}}\,d\zeta \tag{39}$$

$$\hat{D}_m = \int_{-1}^{1} D_0(\xi)\,g_m^*(\xi)\,d\xi \tag{40}$$

$$\hat{D}_{m,n} = \int_{-1}^{1} D_n(\xi)\,g_m^*(\xi)\,d\xi \tag{41}$$

we finally obtain

$$A_{m,n} \approx \left(\frac{b}{p}\right)^2\frac{\pi}{2}\frac{1}{B}\left[\hat{D}_{m,n} - \frac{\hat{D}_m D_n}{D_0}\right]. \tag{42}$$

All of the integrations required in (42) to obtain the explicit expression for $A_{m,n}$ are carried out in the Appendix; (42) then reduces to the *very simple* result

$$A_{m,n} = \frac{1}{B}\left(\frac{b}{p}\frac{\pi}{2}\right)^2 \qquad \text{for all } m, n. \tag{43}$$

IV. Summary and Discussion of the Results Obtained

At this stage we summarize the results obtained so far in the context of the rigorous equivalent network representations presented in Figs. 5 and 6 of Part I. The general network form to be used depends on whether we are describing an aperture or an obstacle; then, the general network form will reduce in different ways depending on whether the discontinuity is "electrically large" (F1 solution) or "eleetrically small" (F2 solution). In addition, the dynamic and static characteristic impedances to be used in the particular network correspond to the TE or TM nature of the excitation.

For the *small-aperture* gratings we employ the general network form shown in Fig. 5 of Part I, where the specific expressions for the network elements follow from the small-argument solutions presented above. *For the small-aperture case with TM excitation*, we have (F1 solution)

$$Z_{m,n} = \frac{(-1)^{m+n+1}}{2B\ln\alpha}\left[1-\alpha^2(m^2+n^2)-2\alpha^2 mn\ln\alpha\right], \qquad m, n = 0\pm1, \pm2, \cdots \tag{44}$$

$$\alpha = \sin\frac{\pi}{2}\frac{a}{p} \tag{45}$$

$$B = j\frac{\omega\epsilon_0 p}{2\pi}\left(\epsilon_r^{(1)} + \epsilon_r^{(2)}\right) \tag{46}$$

$$Y_{n,s}^{(m)} = j\frac{\omega\epsilon_0\epsilon_r^{(m)}p}{2\pi|n|}, \qquad n \neq 0. \tag{47}$$

For the small-aperture case with TE excitation, we have (F2 solution)

$$Z_{m,n} = \frac{1}{B}\left(\frac{a}{p}\frac{\pi}{2}\right)^2 \qquad \text{for all } m, n \tag{48}$$

$$B = \frac{2\pi}{j\omega\mu_0 p}\left(\frac{1}{\mu_r^{(1)}} + \frac{1}{\mu_r^{(2)}}\right) \tag{49}$$

$$Y_{n,s}^{(m)} = \frac{2\pi|n|}{j\omega\mu_0\mu_r^{(m)}p}. \tag{50}$$

For *small-obstacle* gratings we use the general network form given in Fig. 6 of Part I. The series element shown there as $-G_n/(C_r^{(1)} + C_r^{(2)})$ can be renamed $-\bar{G}_n$ for convenience. With this notational modification, we have,

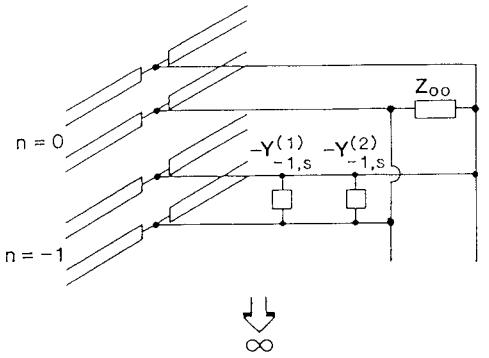

Fig. 4. Because the matrix elements $Z_{m,n}$ in the small-aperture case with TE mode excitation ("electrically small" case) are independent of m or n, the general network description in Fig. 5 of Part I reduces to the very simple one shown here.

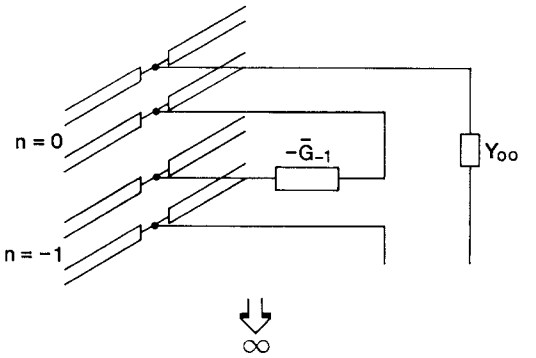

Fig. 5. Because the matrix elements $Y_{m,n}$ in the small-obstacle case with TM mode excitation ("electrically small" case) are independent of m or n, the general network description in Fig. 6 of Part I reduces to the very simple one shown here.

for the small-obstacle case with TM excitation (F2 solution),

$$Y_{m,n} = \frac{1}{B}\left(\frac{d}{p}\frac{\pi}{2}\right)^2 \qquad \text{for all } m, n \tag{51}$$

$$B = \frac{2\pi}{j\omega\epsilon_0 p}\frac{1}{\epsilon_r^{(1)} + \epsilon_r^{(2)}} \tag{52}$$

$$\bar{G}_n = \frac{2\pi|n|}{j\omega\epsilon_0 p}\frac{1}{\epsilon_r^{(1)} + \epsilon_r^{(2)}}. \tag{53}$$

For the small-obstacle case with TE excitation, we have (F1 solution)

$$Y_{m,n} = \frac{(-1)^{m+n+1}}{2B\ln\alpha}\left[1 - \alpha^2(m^2+n^2) - 2\alpha^2 mn\ln\alpha\right]$$
$$\text{for } m, n = 0, \pm 1, \pm 2, \cdots \tag{54}$$

$$\alpha = \sin\frac{\pi}{2}\frac{d}{p} \tag{55}$$

$$B = j\frac{\omega\mu_0 p}{2\pi}\frac{1}{\dfrac{1}{\mu_r^{(1)}} + \dfrac{1}{\mu_r^{(2)}}} \tag{56}$$

$$\bar{G}_n = \frac{j\omega\mu_0 p}{2\pi|n|}\frac{1}{\left(\dfrac{1}{\mu_r^{(1)}} + \dfrac{1}{\mu_r^{(2)}}\right)}. \tag{57}$$

It is important to note that the expressions for $Z_{m,n}$ and $Y_{m,n}$ in (48) and (51), respectively, actually *do not depend on m or n*. As a result of this independence, we can readily show that the relevant networks reduce to the *very simple forms* shown here in Figs. 4 and 5. We first recall, from the definition of the current $\bar{I}_n$ in (8) of Part I, that this current is the actual current in the modal line n when it connects with the box in Fig. 5 of Part I that contains the impedance matrix elements $Z_{m,n}$. The voltage V_m across the modal line m when it connects with that box is then related to all the $\bar{I}_n$ values and the $Z_{m,n}$ terms by relation (9) in Part I, which we repeat here for convenience:

$$V_m = \sum_{n=-\infty}^{\infty} \bar{I}_n Z_{m,n}. \tag{58}$$

Now, since $Z_{m,n}$ in (48) is independent of m or n, it may be called Z_{00} and taken out of the sum in (58). The currents then all add together, and Z_{00} is evidently in parallel across all the modal lines, as we see in Fig. 4. Similar considerations involving (28) and (29) of Part I show that $Y_{m,n}$ of Fig. 6 of Part I may be written as Y_{00}, which is then in series with all the modal lines, as we find in Fig. 5.

Besides their inherent simplicity, one more feature common to all of the network descriptions developed here deserves further comment, namely, that the networks are rapidly convergent with respect to the addition of transmission lines corresponding to further modes. Taking as an example the network shown in Fig. 4, we notice that the two shunt admittances $-Y^{(1)}_{-1,s}$ and $-Y^{(2)}_{-1,s}$ are in parallel with each other and with the transmission lines corresponding to the $n = -1$ modes, and that this combination is in parallel with the coupling element Z_{00}. When $|n|$ becomes large, and when the mode in question is below cutoff, the transmission lines are terminated by their reactive dynamic characteristic admittances $Y_n^{(1)}$ and $Y_n^{(2)}$, which in turn are almost equal to the static characteristic admittances $Y^{(1)}_{n,s}$ and $Y^{(2)}_{n,s}$, since, for TE modes,

$$Y_n^{(m)} = \frac{-j}{\omega\mu_0\mu_r^{(m)}}\left[\left(\frac{2\pi n}{p} + k_{z0}\right)^2 - k_0^2\epsilon_r^{(m)}\mu_r^{(m)}\right]^{1/2}$$

and

$$Y^{(m)}_{n,s} = -j\frac{2\pi|n|}{p\omega\mu_0\mu_r^{(m)}}.$$

The four admittances $Y_n^{(1)}$, $Y_n^{(2)}$, $-Y^{(1)}_{n,s}$, and $-Y^{(2)}_{n,s}$ thus sum to almost zero, so that their shunt effect on Z_{00} is essentially negligible. The contributions from the higher modes thus become vanishingly small as $|n|$ becomes large, permitting us to employ an equivalent network of finite size to represent the discontinuity with sufficient accuracy.

One more issue still needs to be addressed, namely, the range of applicability of the results obtained. In order to obtain an estimate of the range of applicability of the new networks, let us recall that there is a key step common to the approximate solutions of both the F1 and the F2

integral equations, as well as to the derivation of the closed-form analytical expressions for the matrix elements $A_{m,n}$. This key step is the series expansion of the exponential function $\exp[\pm j(2n\pi z)/p]$ on the left-hand side of (1) and (2) and on the right-hand side of (3).

With respect to the solution of the integral equation F2, let us recall the expression for $g_n(\xi)$ in (27) but add one more term in the expansion; we then obtain

$$g_n(\xi) \approx 1 - j\pi\frac{b}{p}n\xi - \frac{1}{2}\left(\pi\frac{b}{p}n\xi\right)^2 + j\frac{1}{3!}\left(\pi\frac{b}{p}n\xi\right)^3 + \cdots. \tag{59}$$

In order to neglect all of the terms above the second order, we must satisfy the following condition:

$$\frac{b}{p} \ll \frac{1}{n}\frac{3}{\pi}. \tag{60}$$

This condition imposes a restriction on the relative geometrical size of the discontinuity in relation to the maximum order of the mode that can be explicitly considered. In fact, (60) shows that if we need to include explicitly a mode of larger order, the admissible relative obstacle or aperture size decreases linearly with increasing order. A similar constraint can be derived from the solution procedure of the F1 integral equation, namely

$$\sin\frac{\pi}{2}\frac{b}{p} \ll \frac{6n}{4n^2-1}. \tag{61}$$

V. Accuracy of the New Simple Networks

In the previous sections we derived two different analytical solutions, which in turn led to new simple equivalent networks, for the scattering problem under investigation. What we need now is a reference solution of proven validity to verify the accuracy of the numerical results obtainable from the simple new networks. Such a reference solution can be obtained by recasting the original boundary-value problem into a Riemann–Hilbert form of known solution [6], which will be referred to from now on as the RH solution. This sophisticated theoretical approach to obtaining accurate numerical solutions to the scattering problem investigated here has already been proposed by other authors (for instance, [7] and [8]), and the accuracy of the numerical results has already been demonstrated.

Using the RH solution given in [7] and the networks developed here, we have performed calculations for several cases and have compared the results obtained. The structure chosen to effect the comparisons is the one shown in Fig. 1, where the angle of incidence θ is 15° and the ratio a/p is varied in the range of small apertures ($a \ll p$) and large apertures, or small obstacles ($a \approx p$). The quantity compared is the relative transmitted power in the lowest mode ($n = 0$ spectral order) versus the relative period p/λ_0. For most of the computations $p/\lambda_0 = 1.70$ is the upper limit of the range evaluated since that range corresponds to the region of interest for the grating application that we originally had in mind (see Fig. 2 of Part I).

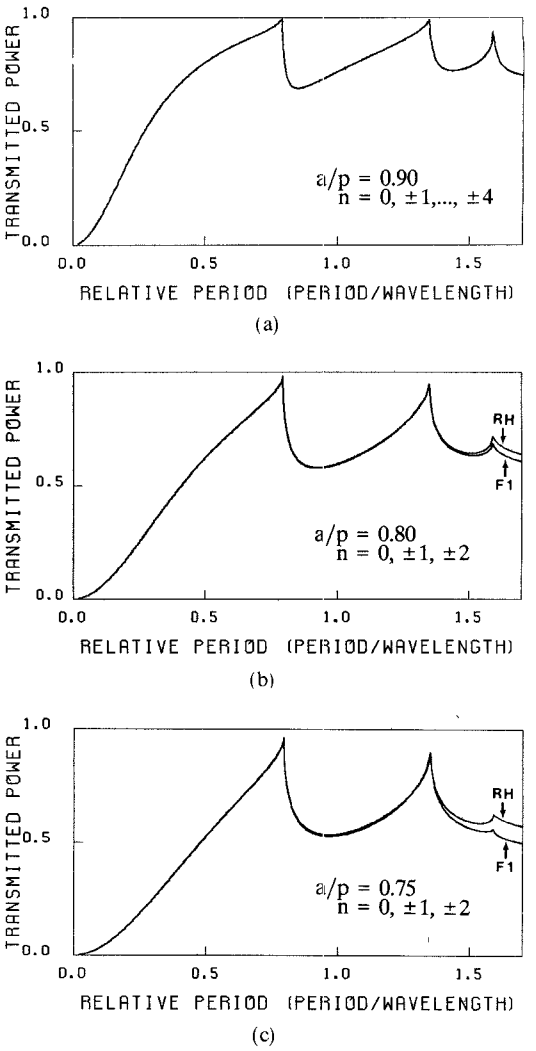

Fig. 6. Comparisons between our F1 solution and the reference (RH) solution for the large-aperture (small-obstacle) range with TE mode incidence ("electrically large" case), for the relative transmitted power in the lowest mode ($n = 0$ spectral order) as a function of the relative period p/λ_0. The angle of incidence (θ in Fig. 1) is 15° and air is present on both sides of the grating. The relative aperture size (a/p in Fig. 1) is equal to 0.9, 0.8, or 0.75 in (a), (b), or (c), respectively. Very good agreement is observed over the range of interest except for case (c), which is at the end of the large-aperture range.

Comparisons are presented below for the case in which there is a dielectric medium ($\epsilon_r^{(2)} = 2.0$) on one side of the grating and air on the other side, as well as for the special case where air is present on both sides.

For the numerical comparisons, we have arbitrarily selected TE excitation; for this excitation, the grating discontinuity will be "electrically small" for small apertures and "electrically large" for small obstacles (or large apertures). For TM excitation, the cases would be reversed but nothing essentially different would arise. Hence the comparisons presented here cover both types of solution and are effectively complete.

Before presenting the numerical results, we should discuss the number of modes that can be included in any specific network representation. We recall first of all that the maximum order n of the modes that can be included is

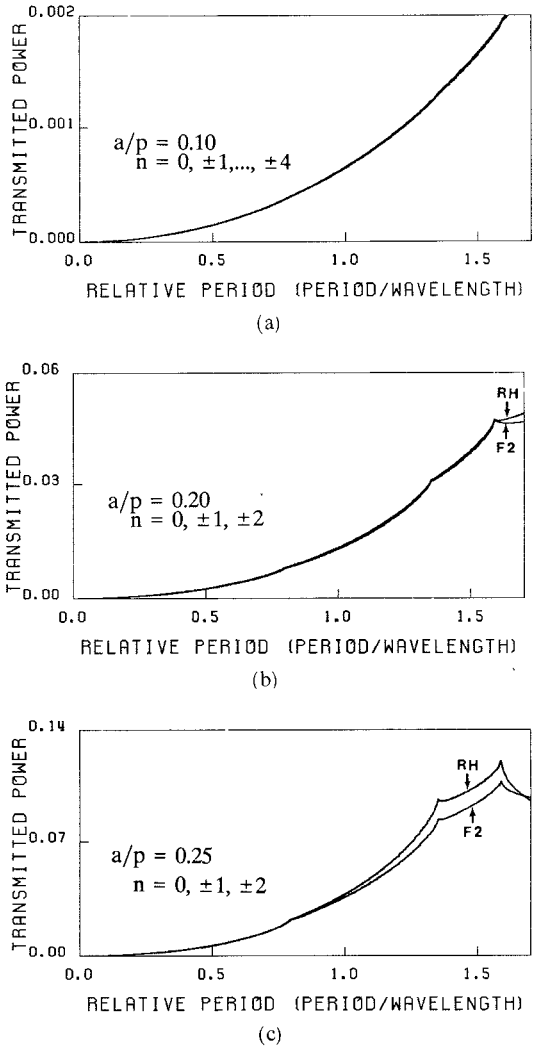

Fig. 7. Comparisons between our F2 solution, employing the simple network in Fig. 4, and the reference (RH) solution for the small-aperture range with TE mode incidence ("electrically small" case), for the relative transmitted power in the lowest mode ($n = 0$ spectral order) as a function of the relative period p/λ_0. All of the structural parameters are the same as those in Fig. 6, except for the relative aperture size a/p, which is equal to 0.1, 0.2, or 0.25 for the cases in (a), (b), or (c), respectively. Very good agreement is observed over the range of interest except for case (c), where we are at the limit of the small-aperture range.

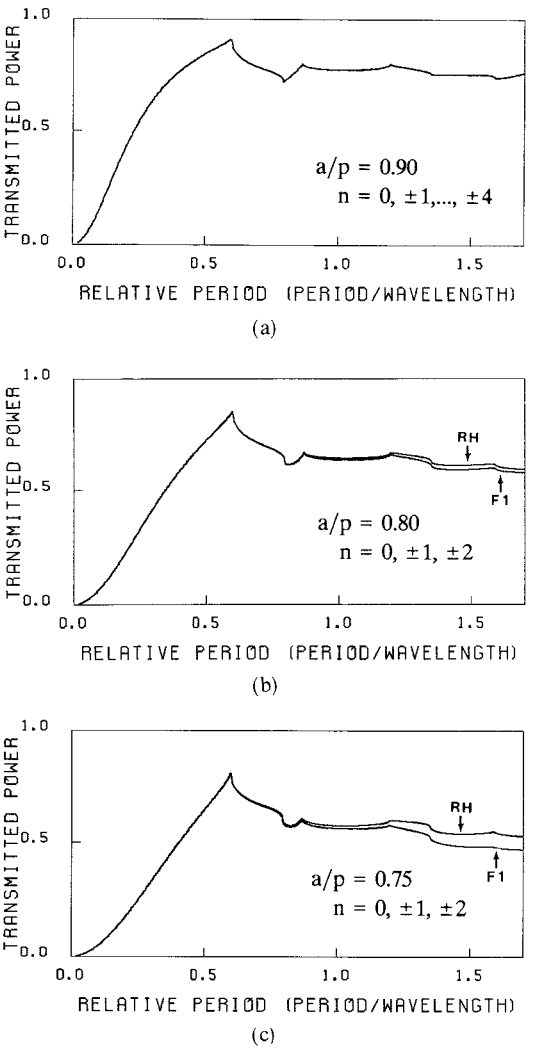

Fig. 8. Same as in Fig. 6 but with a different dielectric medium ($\epsilon_r^{(2)} = 2.0$) on one side of the grating, and air on the other side.

related to the geometry of the grating by condition (60) for electrically small gratings or condition (61) for electrically large ones. For TE excitation and gratings for which a/p is small, condition (60) yields $n \ll 9.5$, 4.8, or 3.8 when $a/p = 0.1$, 0.2, or 0.25, respectively. To loosely satisfy condition (60), the largest value of n that we could select in these three cases would be $n = \pm 4$, ± 2, or ± 2. For the range of large apertures, condition (61) is not as direct, but similar considerations would permit us to choose n up to ± 4, ± 2, or ± 2 for $a/p = 0.9$, 0.8, or 0.75, respectively. These are the values we have chosen for our numerical comparisons.

A limitation in the mode number n also limits the range of p/λ_0 over which the network representation is valid. As p/λ_0 is increased, a larger number of modes go above cutoff, and they must be included explicitly in the network representation. When this requirement conflicts with conditions (60) or (61), we have reached the limit in the range of p/λ_0 for which the network representation can yield accurate numerical results. Since n can be chosen up to ± 4 for $a/p = 0.9$ as compared with ± 2 for $a/p = 0.8$, for example, we should expect that the results for $a/p = 0.9$ would be accurate over a much larger range of p/λ_0. Furthermore, since higher modes begin to radiate at lower frequencies in a dielectric medium than in air, if a dielectric medium is present on one side of the grating the same maximum mode order would result in a somewhat smaller range of p/λ_0. We shall see below that such behavior is borne out by our numerical results.

With this introduction we are now ready to present the numerical comparisons. Fig. 6 shows the results obtained for a symmetric case ($\epsilon_r^{(1)} = \epsilon_r^{(2)} = 1.0$) in the large relative aperture (or small-obstacle) range, namely $a/p = 0.9$, 0.8, and 0.75 for the cases in (a), (b), and (c), respectively. In accordance with condition (61), the numbers of modes we have included in the networks are $n = \pm 4$, ± 2, and ± 2, respectively. As we can see, the agreement with the RH solution is excellent over the range of interest except for

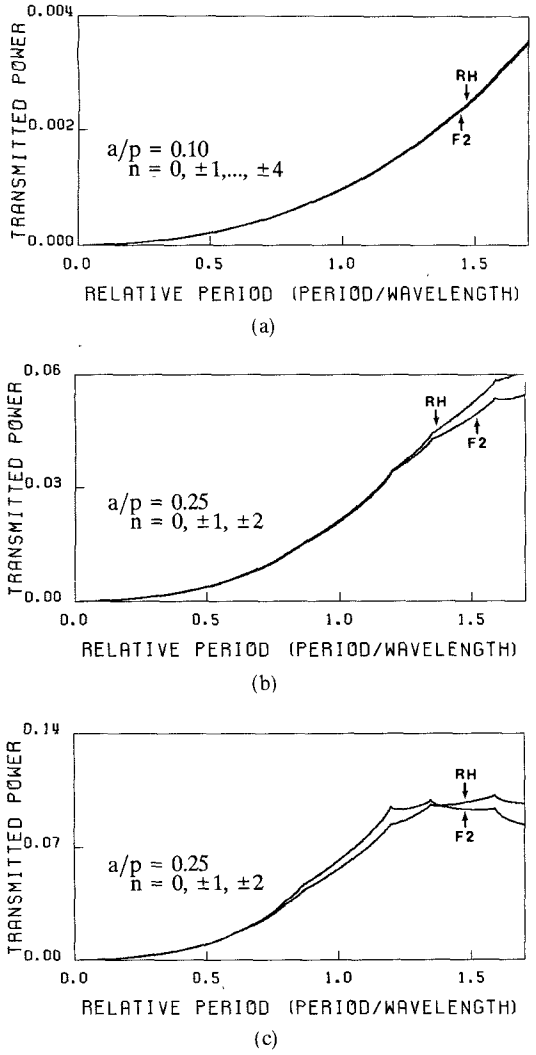

Fig. 9. Same as in Fig. 7 but with a different dielectric medium ($\epsilon_r^{(2)} = 2.0$) on one side of the grating, and air on the other side.

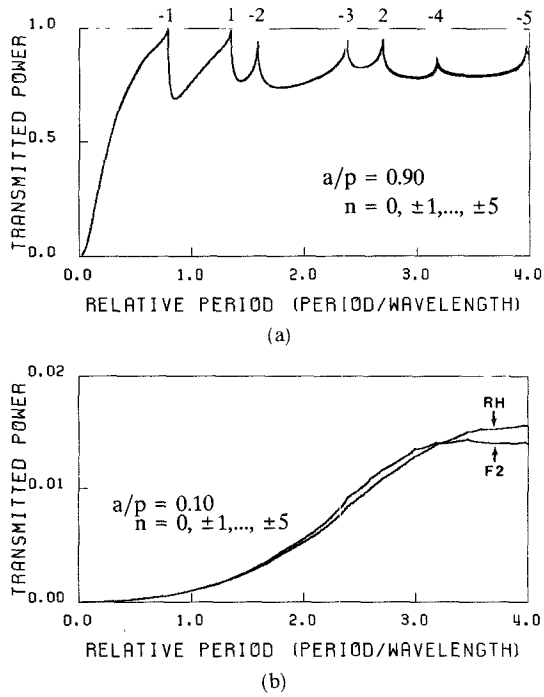

Fig. 10. For this set of comparisons we have explicitly included in the networks higher order modes up to $n = \pm 5$, and we have extended the relative period range up to $p/\lambda_0 = 4.0$. The case in (a) corresponds to $a/p = 0.9$ with air on both sides of the grating, while case (b) corresponds to $a/p = 0.1$ with $\epsilon_r^{(1)} = 1.0$ and $\epsilon_r^{(2)} = 2.0$. When these new networks are used well within their respective ranges of validity, they are very accurate and, at the same time, can accommodate a substantial number of propagating higher modes (or spectral orders).

the case in (c), where we are at the limit of validity for the large-aperture condition. (The curves are direct computer plots, and in Fig. 6(a) the two different solutions are coincident.) Fig. 7 presents the comparisons obtained for the same parameters as for Fig. 6, but in the small-aperture range, namely $a/p = 0.1$, 0.2, and 0.25 for the cases in (a), (b), and (c), respectively. (Note that the ordinate scales are different for cases (a), (b), and (c) in Fig. 7.) As mentioned above, the numbers of modes included in the networks for these computations are $n = \pm 4$, ± 2, and ± 2, in accordance with (60). Again, we observe very good agreement over most of the range of interest, but the results obtained from the network for case (c) are seen to deteriorate since we are at the end of the small-aperture range.

In both sets of figures we observe the presence of sharp peaks at specific values of p/λ_0. These peaks occur when a higher mode just reaches cutoff in the x direction, corresponding to a diffracted beam which is just at the grazing angle in the z direction. The peaks are also the same as the pure Rayleigh form of Wood's anomalies. Going in the direction of increasing p/λ_0 values in Fig. 6(a), the first, second, and third peaks occur when the $n = -1$, $+1$, and -2 modes, respectively, are exactly at cutoff. The peaks in Fig. 6 are much more pronounced than those in Fig. 7 because the grating for the calculations in Fig. 6 represents an electrically large discontinuity.

Figs. 8 and 9 exhibit the results found for the same set of parameters as those used for Figs. 6 and 7, respectively, but with a different dielectric medium (with $\epsilon_r^{(2)} = 2$) on one side of the grating. As we can see, the same general pattern of agreement with the RH solution is obtained. We also recognize that the presence of the dielectric medium reduces the range of p/λ_0 over which good agreement is expected, in accordance with the discussion above. Note again the presence of peaks in both Figs. 8 and 9, corresponding to values of p/λ_0 at which progressively higher order modes are at cutoff in the air or in the dielectric region.

Finally, in accordance with the discussion above, we demonstrate in Fig. 10(a) and (b) that when a higher number of modes can be included in the appropriate network, according to conditions (60) or (61), accurate results can be expected over a larger range of p/λ_0. We included modes up to ± 5 in the networks corresponding to $a/p = 0.1$ and 0.9. We observe from Fig. 10(a), for $a/p = 0.9$, that the agreement with the RH solution is excellent up to $p/\lambda_0 = 4.0$. At the top of the figure we indicate the correlation between the cusp peak and the order n of the higher mode that just begins to propagate,

and we note that the $n=-5$ mode begins to propagate at p/λ_0 almost equal to 4.0. Since the $n=-6$ mode is not included in the network, we would not expect the excellent agreement to continue much above $p/\lambda_0=4.0$. For Fig. 10(b), which corresponds to $a/p=0.1$ and different dielectrics on each side of the grating, the discrepancy between the two curves occurs earlier, i.e., for lower values of p/λ_0, mainly because the higher modes begin to propagate on the dielectric side at lower values of p/λ_0. Although the RH reference solution is accurate over a larger range of p/λ_0 values than is our network solution, we should add that the computation time required for the RH solution is far greater, particularly as more modes are added, since a matrix inversion is required. A prime virtue of our small-argument solutions is their relative simplicity.

VI. Conclusions

Many valuable papers have been published that are concerned with the scattering of a plane wave by a periodic metal-strip grating. Some papers provide accurate numerical results even in the general case of arbitrary angle of incidence, TE or TM field polarization, arbitrary strip-to-period ratios, and, more important, a different medium on each side of the grating and period-to-wavelength ratios that permit diffracted higher order beams to be present (multimode situation). Although procedures that provide purely numerical results are available, comparable useful equivalent network representations do not exist.

In Part I of this pair of papers we present two new rigorous multimode equivalent network representations that are valid for the general situation indicated above. These two new network representations, based on aperture and obstacle formulations, respectively, follow from a rephrasing of the relevant integral equations in which "static" kernels are employed. The resulting integral equations remain rigorous, and so do the new network representations that follow from them, despite the simplified nature of the kernels, which in fact make it easier for us to derive analytical solutions. Application to either TE or TM excitation follows directly upon the insertion of the appropriate expressions for the modal characteristic impedance. It is then shown that of the four cases (aperture or obstacle formulation with TE or TM excitation), only two basically different types of integral equation result; they are both Fredholm integral equations of the first kind with singular "static" kernels, but the kernels in each are different. The two different integral equations are then identified as corresponding to "electrically large" (F1) and "electrically small" (F2) formulations of the grating discontinuity.

In Part II, these two integral equations are solved in the small-argument limit, yielding very simple analytical expressions for the elements of the equivalent networks, which are then valid for the small-aperture and the small-obstacle dimensional ranges. The equivalent networks themselves simplify greatly, and those for the "electrically small" case become strikingly simple.

For the wonderful advantage of having such very simple network forms with analytically very simple expressions for the network elements, we pay a price. The price is that only a limited number of modes can be included in the networks, in accordance with conditions (60) or (61). If that limit is exceeded, the networks become less valid (in addition to becoming slightly more complicated). In practice, this means that the range of aperture-to-period (a/p) is limited to values below 0.25 or above 0.75, and that the p/λ_0 values are also correspondingly limited (depending on the number of modes permitted in the networks). Within this limited, but not so small, range of grating strip dimensions and wavelengths, we now have available an ultrasimple group of equivalent networks which provide very good accuracy. Five sets of curves are presented which illustrate the accuracy obtained.

The importance of these equivalent networks resides in their inherent simplicity and flexibility, which makes them powerful tools for the analysis of more complex structures containing these gratings as constituents.

Appendix
Evaluation of Integrals Occurring in the Singular Integral Equation Solution

Before describing the analytical evaluation of the integrals in question, it is appropriate to introduce some results that will be useful later, namely,

$$\sum_{n=0}^{N}\xi^n\zeta^{N-n}=\frac{\zeta^{N+1}-\xi^{N+1}}{\zeta-\xi} \tag{A1}$$

$$\frac{1}{\pi}\fint_{-1}^{1}\frac{\sqrt{1-\zeta^2}}{\zeta-\xi}\,d\zeta=-\xi \qquad \text{for } |\xi|\leqslant 1. \tag{A2}$$

Equation (A1) can be simply derived from the partial power series of (ξ/ζ), and the derivation of (A2) can be found in [5]. We can now proceed with the evaluation of the integrals, starting with $G_n(\xi)$, which we will rewrite explicitly, using (34) and (27):

$$\begin{aligned}G_n(\xi)=&\frac{1}{\pi}\fint_{-1}^{1}\frac{\sqrt{1-\zeta^2}}{\zeta-\xi}\,d\zeta\\&-j\pi\frac{b}{p}n\frac{1}{\pi}\fint_{-1}^{1}\frac{\sqrt{1-\zeta^2}}{\zeta-\xi}\zeta\,d\zeta\\&-\frac{1}{2}n^2\left(\pi\frac{b}{p}\right)^2\frac{1}{\pi}\fint_{-1}^{1}\frac{\sqrt{1-\zeta^2}}{\zeta-\xi}\zeta^2\,d\zeta.\end{aligned} \tag{A3}$$

The first integral in (A3) is the same as (A2); using (A1), the second and third integrals can be reduced to a combination of integrals similar to the one in (A2) and other known integrals. We finally obtain

$$G_n(\xi)=-\xi-j\pi\frac{b}{p}n\left(\frac{1}{2}-\xi^2\right)-\frac{n^2}{2}\left(\pi\frac{b}{p}\right)^2\left(\frac{\xi}{2}-\xi^3\right). \tag{A4}$$

The evaluation of $D_n(\xi)$ is now straightforward, yielding

$$D_n(\xi) = \int_{-1}^{\xi} \frac{G_n(\zeta)}{\sqrt{1-\zeta^2}}\, d\zeta$$

$$= \sqrt{1-\xi^2}\left[1 - jn\pi\frac{b}{p}\frac{\xi}{2} - \frac{1}{4}n^2\pi^2\left(\frac{b}{p}\right)^2\right]$$

$$+ \frac{1}{6}n^2\pi^2\left(\frac{b}{p}\right)^2(1-\xi^2). \tag{A5}$$

Note also that from (A5) we have

$$D_n(1) = D_n = 0 \tag{A6}$$

and, therefore, to evaluate $A_{m,n}$ we only need $\hat{D}_{m,n}$. To evaluate this quantity we now need to integrate the following expression:

$$\hat{D}_{m,n} = \int_{-1}^{1} D_n(\xi)\, g_m^*(\xi)\, d\xi \tag{A7}$$

which, after a few simple steps, becomes

$$\hat{D}_{m,n} = \frac{\pi}{2}. \tag{A8}$$

ACKNOWLEDGMENT

The authors wish to thank Prof. J. G. Encinar, Grupo de Electromagnetismo Aplicado, Universidad Politecnica de Madrid, Madrid, Spain, for his significant contribution to the assessment of the range of validity of the small-argument solutions, and Prof. H. Hochstadt of the Mathematics Department of Polytechnic University for his valuable comments on various mathematical aspects.

REFERENCES

[1] I. Palocz and A. A. Oliner, "Equivalent network of a multimode planar grating," *IEEE Trans. Microwave Theory Tech.*, vol. MTT-18, pp. 244–252, May 1970.

[2] N. Marcuvitz, *Waveguide Handbook* (MIT Radiation Laboratory Series). New York: McGraw-Hill, 1951, pp. 146–152.

[3] F. Oberhettinger, *Fourier Expansions a Collection of Formulas*. New York: Academic Press, 1973.

[4] J. Schwinger and D. Saxon, *Discontinuities in Waveguides*. New York: Gordon and Breach, 1968, p. 72.

[5] L. Lewin, *Theory of Waveguides*, New York: Wiley, 1975, p. 201.

[6] N. I. Muskhelishvili, *Singular Integral Equations*, 2nd ed. Institute of Mathematics, Tifilis USSR, 1946.

[7] Z. S. Agronovich, V. A. Marchenko, and V. P. Shestopalov, "The diffraction of electromagnetic waves from plane metallic lattices," *Sov. Phys.—Tech. Phys.*, vol. 7, no. 4, pp. 227–286, Oct. 1962.

[8] A. M. Barbosa, A. S. dos Santos, and J. Figanier, "Wave propagation on a strip grating over an impedance plane. Solution by reduction to a modified Riemann-Hilbert problem," *Radio Sci.*, vol. 18, no. 18, pp. 519–531, July–Aug. 1983.

[9] G. L. Baldwin and A. E. Heins, "On the diffraction of a plane wave by an infinite plane grating," *Math. Scand.*, vol. 2, pp. 103–118, 1954.

Marco Guglielmi was born in Rome, Italy, on December 17, 1954. He received the degree "Laurea in Ingegneria Elettronica" in 1979 from the University of Rome "La Sapienza," Rome, Italy, where in 1980 he also attended the "Scuola di Specializzazione in Elettromagnetismo Applicato." In 1981 he was awarded a Fulbright Scholarship in Rome and an HISP scholarship (Halsey International Scholarship Program) from the University of Bridgeport, Bridgeport, CT, where in 1982 he obtained the M.S. degree in electrical engineering. In 1986 he received the Ph.D. degree in electrophysics from the Polytechnic University, Brooklyn, NY. From 1984 to 1986 he was an Academic Associate at the Polytechnic University, and since 1986 he has been an Assistant Professor in the Electrical Engineering Department there.

In 1987 Dr. Guglielmi was the second prize winner of the URSI National Student Paper Prize Competition in Boulder, CO. His professional interests include the areas of solid-state devices and circuits, microwave active and passive devices, network representations of waveguide discontinuities, periodic structures, phased arrays, and millimeter-wave leaky-wave antennas.

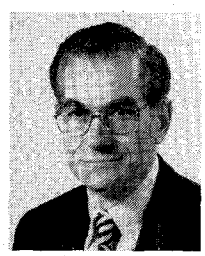

Arthur A. Oliner (M'47–SM'52–F'61–LF'87) was born in Shanghai, China, on March 5, 1921. He received the B.A. degree from Brooklyn College, Brooklyn, NY, and the Ph.D. degree from Cornell University, Ithaca, NY, both in physics, in 1941 and 1946, respectively.

While at Cornell University, he held a Graduate Teaching Assistantship in the Physics Department and also conducted research on a project of the Office of Scientific Research and Development. He joined the Microwave Research Institute of the Polytechnic Institute of Brooklyn, Brooklyn, NY, in 1946, and was made Professor in 1957. From 1966 to 1971, he was Head of the Electrophysics Department; he then became Head of the combined Department of Electrical Engineering and Electrophysics from 1971 through 1974. He was also the Director of the Microwave Research Institute from 1967 to 1981. During the summer of 1964, he was a Walker–Ames Visiting Professor at the University of Washington, Seattle, and during the 1965–1966 academic year he was on sabbatical leave at the Ecole Normale Supérieure, Paris, France, under a Guggenheim Fellowship. During the summer of 1973, he was a Visiting Professor at the Catholic University, Rio de Janeiro, Brazil; in the spring of 1978 he was a Visiting Research Scholar at the Tokyo Institute of Technology, Japan; in the spring of 1980 he was a Visiting Professor at the Huazhong (Central China) Institute of Technology, Wuhan, China; and in the fall of 1982 he was a Visiting Professor at the University of Rome "La Sapienza," Rome, Italy. He has been engaged in research in a wide variety of topics in the microwave field, including network representations of microwave

structures, precision measurement methods, guided-wave theory with stress on surface waves and leaky waves, traveling-wave antennas, plasmas, periodic structure theory, and phased arrays. His interests have also included waveguides for surface acoustic waves and integrated optics and, more recently, guiding and radiating structures for the millimeter and near-millimeter wave ranges. He is the author of more than 180 papers, and coauthor or coeditor of three books. He served on the Editorial Boards of the journal *Electronics Letters* (published by the British IEE) and the volume series *Advances in Microwaves* (Academic Press).

Dr. Oliner is a Fellow of the AAAS and the British IEE, and he served as the first MTT National Lecturer in 1967. He has received prizes for two of his papers: the IEEE Microwave Prize in 1967 and the Institution Premium, the highest award of the British IEE, in 1964. He was named an Outstanding Educator of America in 1973, and in 1974 he received a Sigma Xi Citation for Distinguished Research. He was a National Chairman of the IEEE MTT Society, a member of the IEEE Publication Board, and General Chairman of three symposia. In 1977 he was elected an Honorary Life Member of the IEEE MTT Society, and in 1982 he received the IEEE Microwave Career Award. In 1984, he was a recipient of the IEEE Centennial Medal. He is a member of several Commissions of the International Union of Radio Science (URSI), a past Chairman of Commission 1 (now A), and a past USA Chairman of Commission D. He is also a former Chairman of a National Academy of Sciences Advisory Panel to the National Bureau of Standards.